IOP Conf. Series: Materials Science and Engineering **276** (2017) 012012 doi:10.1088/1757-899X/276/1/012012

Study of lifting operation of a tripod foundation for offshore wind turbine

H Zhu, L Li* and M C Ong

Department of Mechanical and Structural Engineering and Materials Science
University of Stavanger, Stavanger, Norway

*Corresponding author: lin.li@uis.no

Abstract. This study addresses numerical analysis of the installation of a tripod foundation using a heavy lift vessel (HLV). Limiting sea states are firstly predicted in the frequency domain based on crane tip vertical motions using linear transfer functions. Then, numerical modelling and simulations are carried out in the time domain to analyse the coupled dynamic system taking into consideration of the nonlinearities of the system. In time-domain analysis, two lifting phases are brought into focus, i.e., the lift-off and the lowering phases. For the lift-off phase, two scenarios are considered, i.e., lift-off from the own deck of the HLV and lift-off from a transport barge. Moreover, comparative studies using two types of installation vessels, a floating vessel and a Jack-up, are investigated for the lowering process. Critical responses including the motions of the tripod and the lift wire tensions are presented and compared under various environmental and loading conditions.

1. Introduction

The installation of offshore wind farms continues to increase, which is driven by many factors. The potential energy produced from wind is proportional to the cube of the wind speed. As a result, only a small increment of the wind speed can produce a significantly larger amount of electricity. Compared to the wind plants on land, higher wind speed and low turbulence intensity offshore can result in up to 50% higher energy production [1]. Since more wind energy can be captured offshore, together with other positive factors, such as technology transfer from oil and gas industry, offshore wind industry has boomed around the world, especially in European countries around the North Sea and the Baltic Sea. It is predicted that offshore wind will provide a growing share and reach one third all the wind generated energy by 2050 [2].

Marine lifting operations play a key role in the installation of offshore wind turbines (OWTs) and their bottom-fixed foundations. The installation of OWT monopile support structures has been investigated in some research work through numerical modelling and analysis [3]. The lifting operations are typically carried out by a floating or a jack-up crane vessel. Compared to the jack-up vessel which stands still on the sea bed, the motions of the floating vessel would affect motion responses of the lifted object which is a tripod foundation in the present study. However, floating vessels with onboard heavy cranes are more efficient than the jack-up for mass installations of a wind farm, thanks to their fast transit among the locations of the turbines.

In this paper, lifting operations of a tripod foundation using a heavy lift vessel (HLV), are studied. To author's knowledge, there are limited publications available in open literature, which address the

numerical simulation of a tripod foundation. Investigation is first carried out in the frequency domain. Based on the linear wave theory and linear response process [4], wave induced rigid body motions of the vessel alone are calculated. Concerning critical response parameters, limiting sea states are predicted based on probabilistic acceptance criteria [5]. Then, time domain simulations are performed for the coupled dynamic lifting system of the HLV and the tripod. The predicted limiting sea states using the frequency domain method are cross checked in the time domain by running stationary simulations. Attentions are consequently devoted to two time-varying non-stationary processes, i.e., the lowering phase and the lift-off phase. Potential critical events, such as snap load in the lift wire, collision with the lifting vessel or even re-hit during the lift-off phase, are studied. Installation system and theoretical background are introduced first, ahead of the limiting sea states prediction in the frequency domain. Then, clarifications on the numerical modelling are presented prior to the analysis and discussion of the time domain simulation results. In the end, conclusions and future work are listed.

2. Installation system

The weight of a tripod foundation which depends on the capacity of the wind turbine and the water depth, can reach hundreds of tons. In this study, a tripod weighing 920 tons [6] is used and the main parameters are shown in Table 1. Due to the heavy weight and the bulky size of the tripod foundation, a heavy lift floating vessel is chosen for the installation. The main dimensions of the HLV [7] can also be found in Table 1.

Table 1. Main parameters of the HLV and the tripod foundation.

Vessel (HLV)		**Tripod**	
Item	**Value**	**Item**	**Value**
Length overall [m]	183	Total mass [tons]	920
Breadth [m]	47	Total height [m]	63
Moulded depth [m]	18.2	Outer diameter (central column) [m]	5.7
Operational draught [m]	10.2	Outer diameter (braces) [m]	1.2 - 3.15

The onboard crane is capable to perform lifting operation up to 5000 tons with maximum 100 m lifting height from its freeboard deck. The positioning system of the HLV allows for lifting operations in close proximity to other structures, such as lift-off operation of the tripod from a transport barge. For the lifting operation, the position of the crane tip plays a crucial role for the limiting sea states prediction since the crane tip motions are considered as critical responses. Moreover, the motions of the crane tip affect the response of the coupled dynamic lifting system. Hence, the crane tip position should be decided based on the general arrangement of the HLV and the technical specification of the onboard crane.

The global coordinate system is a right-handed coordinate system with the X-axis pointing towards the bow, the Y-axis towards the port side and the Z-axis pointing upwards. The origin of the global coordinate system is located on the ship's centerline, at the cross of the midship section and the still water level during the lifting operation. In addition, the body fixed coordinate system (moving with the body) of the HLV coincides with the global coordinate system when the HLV is at rest. In this study, the coordinates of the crane tip are chosen as $x_p = -81.7\,m,\ y_p = 53.5m, z_p = 88\,m$, relative to the origin of the body fixed coordinate system of the HLV. Moreover, the origin of the body-fixed coordinate of the tripod in the numerical model is set on the axis of its central column, at the point 18m beneath the top of the column (45 m above the lower tip). Figure 1 shows the schematic lifting arrangement of the tripod in the global coordinate system.

In the present study, the offshore site North Sea Centre (Site No. 15) [8] is chosen as a reference installation site. Typical wave conditions from this site would be used as input for the analysis.

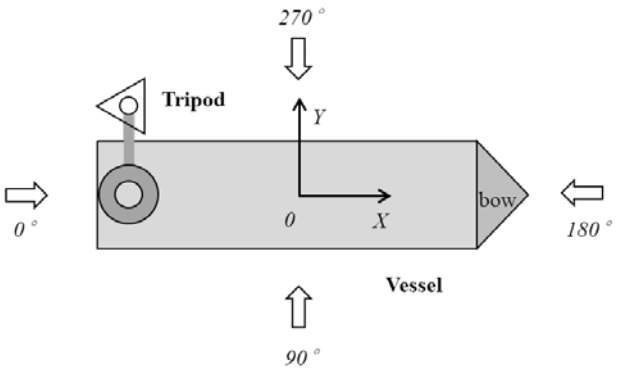

Figure 1. Lifting arrangement of the tripod in the global coordinate system.

3. Theoretical background

3.1. Motions and responses

For the crane tip with the coordinates (x_p, y_p, z_p) in the body fixed coordinate system of the HLV, the motions of the point can be expressed in the following equation [9]:

$$\boldsymbol{s} = \left(\eta_1 + \mathrm{z_p}\eta_5 - \mathrm{y_p}\eta_6\right)\boldsymbol{i} + \left(\eta_2 - \mathrm{z_p}\eta_4 + x_\mathrm{p}\eta_6\right)\boldsymbol{j} + (\eta_3 + \mathrm{y_p}\eta_4 - \mathrm{x_p}\eta_5)\boldsymbol{k} \tag{1}$$

where, $\boldsymbol{i}$, $\boldsymbol{j}$ and $\boldsymbol{k}$ are the unit vectors and η_1 through η_6 are the rigid body motions of the vessel in surge, sway, heave, roll, pitch and yaw respectively. The crane tip vertical motion is thus formulated as:

$$\boldsymbol{s}_v = \eta_3 + \mathrm{y_p}\eta_4 - \mathrm{x_p}\eta_5 \tag{2}$$

besides the heave motion η_3, the vertical motion of the crane tip is also affected by the vessel roll η_4 and the vessel pitch η_5. In addition, the positions of the crane tip also affect the vertical motion.

In general, transfer function encompasses both the amplitude scaling and phase shift of the response relative to the wave component. For each degree of freedom, the function can be expressed in complex:

$$H_i(\omega) = A_i(\omega)\exp(i\varphi_i(\omega)) \tag{3}$$

where, $H_i(\omega)$, the transfer function in the i-th degree of freedom; $A_i(\omega)$, amplitude of the transfer function, also denoted as response amplitude operator (RAO) which gives the ratio between the response amplitude to the wave amplitude; $\varphi_i(\omega)$, phase angle of the transfer function; ω, angular frequency of interest.

Given the transfer functions of the vessel, the wave induced rigid body motions at the crane tip can be calculated through motions superposition as in equation (1). For crane tip vertical motion, it can be shown as:

$$\begin{aligned}\boldsymbol{s}_v = \eta_3 + \mathrm{y_p}\eta_4 - \mathrm{x_p}\eta_5 &= H_3(\omega)\cdot\,\zeta_a + \mathrm{y_p}H_4(\omega)\cdot\,\zeta_a - \mathrm{x_p}H_5(\omega)\cdot\,\zeta_a \\ &= \left[H_3(\omega) + \mathrm{y_p}H_4(\omega) - \mathrm{x_p}H_5(\omega)\right]\cdot\,\zeta_a\end{aligned} \tag{4}$$

where, ζ_a is the wave amplitude while the part, $H_3(\omega) + \mathrm{y_p}H_4(\omega) - \mathrm{x_p}H_5(\omega)$, is combined transfer function for the crane tip vertical motion, denoted as $H_v(\omega)$. By substituting equation (3), it can be further expressed as:

$$\begin{aligned}H_v(\omega) = H_3(\omega) + \mathrm{y_p}H_4(\omega) - \mathrm{x_p}H_5(\omega) &= A_3(\omega)\exp\left(i\varphi_3(\omega)\right) + y_p\cdot A_4(\omega)\exp\left(i\varphi_4(\omega)\right) \\ &\quad -x_p\cdot A_5(\omega)\exp(i\varphi_5(\omega))\end{aligned} \tag{5}$$

The calculation of the crane tip vertical motion can be further conducted, ended in the form of response spectrum as in equation (6) and spectral moment as in equation (7).

$$S_R(\omega) = |H_v(\omega)|^2 S(\omega) = [RAO(\omega)]^2 S(\omega) \quad (6)$$

$$m_n = \int_0^\infty \omega^n S_R(\omega)\, d\omega \quad (7)$$

where, RAO is the absolute value (amplitude) of the combined transfer function, S_R is the response spectrum, S is the wave spectrum, ω is the wave angular frequency and m_n is the response spectral moment of general order n.

Response variance σ_R^2, equal to the zeroth response spectral moment, can be expressed as:

$$\sigma_R^2 = m_0 = \int_0^\infty S_R(\omega)\, d\omega \quad (8)$$

Average zero-up-crossing period for the response, T_z, can then be estimated by:

$$T_z = 2\pi \sqrt{\frac{m_0}{m_2}} \quad (9)$$

Consequently, number of response cycles in 1-hour, n_{1h}, can be formulated as:

$$n_{1h} = N = \frac{3600}{T_z} \quad (10)$$

3.2. Limiting sea states based on the critical crane tip motion

Since lifting operations take place in relatively calm weather, the motions of the crane vessel can be computed from linear wave theory and the motions can be assumed to be Gaussian distributed [10] and the global maxima (largest maximum between adjacent zero-up-crossings) follows a Rayleigh distribution [11]. The distribution of 1-hour global response maxima can be expressed as equation (11), by assuming the global maxima in 1-hour as statistically independent and identically distributed.

$$F(X) = \left\{1 - exp\left\{-\frac{1}{2}\left(\frac{X}{\sigma}\right)^2\right\}\right\}^{n_{1h}} \quad (11)$$

where, σ is the standard deviation of the response.

The maximum vertical motion of the crane tip in one hour (Z_{1h}) is chosen as the critical parameter for the lifting operation. Based on limiting criteria with the limiting value Z_{lim}, the probability of exceedance (with $Z_{1h} > Z_{lim}$), can be shown as:

$$P[Z_{1h} > Z_{lim}] = 1 - \left\{1 - exp\left\{-\frac{1}{2}\left(\frac{Z_{\lim}}{\sigma_z}\right)^2\right\}\right\}^N \quad (12)$$

where, σ_z is the standard deviation of crane tip vertical motion. The probability of exceedance is a measurement of risk taken for the marine operation. Low probability of exceedance is preferred for relatively safe operation. In practice, the acceptable probability of exceedance (acceptance criteria) depends on the cost and consequences due to the failure. Given the acceptance criteria (allowable probability of exceeding the limiting value), q_{1h}, the marine operation can only be conducted satisfying the condition as in equation (13).

$$1 - \left\{1 - exp\left\{-\frac{1}{2}\left(\frac{Z_{\lim}}{\sigma_z}\right)^2\right\}\right\}^N \leq q_{1h} \quad (13)$$

Equation (13) can be transformed as:

$$\sigma_z \leq \frac{Z_{lim}}{\sqrt{-2\ln[1-(1-q_{1h})^{1/N}]}} \quad (14)$$

Since the motion standard deviation is a function of the sea state (H_s and T_p), the limiting H_s (significant wave height) and T_p (spectral peak period), can be found as:

$$\sigma_{z,lim}(H_s, T_p) = \frac{z_{lim}}{\sqrt{-2\ln[1-(1-q_{1h})^{1/N}]}} \quad (15)$$

4. Prediction of limiting sea states in the frequency domain

4.1. RAOs of the crane tip vertical motion

Based on the motion transfer functions of the vessel, the RAOs of the crane tip vertical motion can be calculated by referring to equation (5) and they are presented in Figure 2.

It can be found from the figure that the RAO values vary significantly with the wave directions and the lowest occurs in the head sea (180deg). Besides, the curves in various wave directions peak at the frequency around 0.4 rad/s which is close to the natural frequency of the vessel roll.

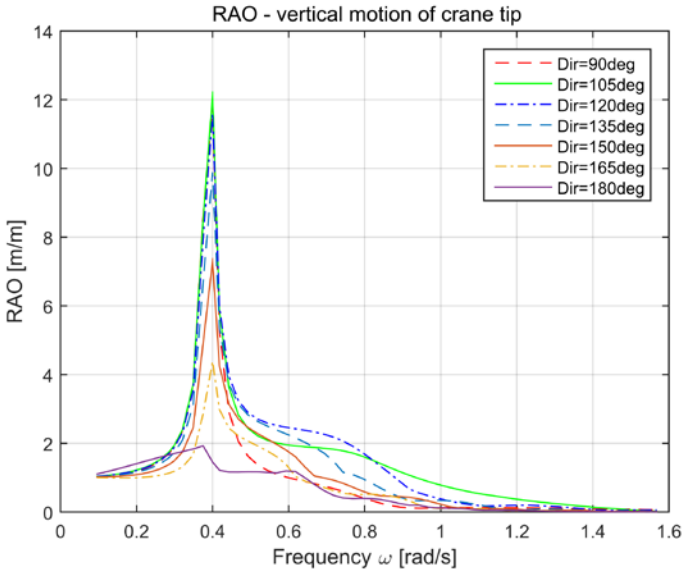

Figure 2. RAOs of the crane tip vertical motion.

4.2. Response spectrum of crane tip vertical motion

The response spectrum of the crane tip vertical motion was calculated from equation (6) using long crested JONSWAP wave spectrum for the reference site. Two wave conditions ($H_s = 1.25m$ and $H_s = 2.5m$ at $T_P = 7s$) with relatively high probability of occurrence according to the 10-year scatter diagram [12], were selected, together with the third one ($H_s = 2.5m$ and $T_P = 16s$) for comparison. In addition to the chosen position for the crane tip, one virtual position (Position 2, closer to the center of gravity of the HLV in X direction) is also used to study the influence from the varied crane tip positions. Coordinates of the crane tip positions are shown in Table 2. Although the assumed Position 2 is practically impossible to reach due to the limited working radius of the onboard crane, the comparative study illustrates the significant influences of crane tip location on the crane tip motions.

Table 2. Coordinates of the crane tip during installation.

Coordinates of crane tip	X	Y	Z
Position 1 (the chosen)	-81.7	53.5	88
Position 2 (the virtual)	-10.5	53.5	88

Figure 3 presents the response spectra of the crane tip vertical motion under the three wave conditions. Huge differences can be observed using different crane tip positions as shown in the Figure 3 (a) and (b). The peak values of the response spectra in the wave direction of 105deg and 120deg using Position 1 is remarkably larger than those using Position 2 which is much closer to the center of gravity (CoG) of the vessel. It demonstrates that the crane tip motions can be greatly mitigated by reasonably locating the crane tip toward mid-ship during installation operation. While, for the wave condition with

$T_p = 16s$ as shown in Figure 3 (c), the differences using the two crane tip positions are minor. The peak values for both cases are extremely high due to resonance. The resonance occurs because the spectral peak period (16s) of the JONSWAP wave spectrum is close to the natural period of the roll motion of the HLV. Moreover, the HLV should better be oriented against the incoming wave (165deg or 180deg) during the operation to avoid large roll induced crane tip motions.

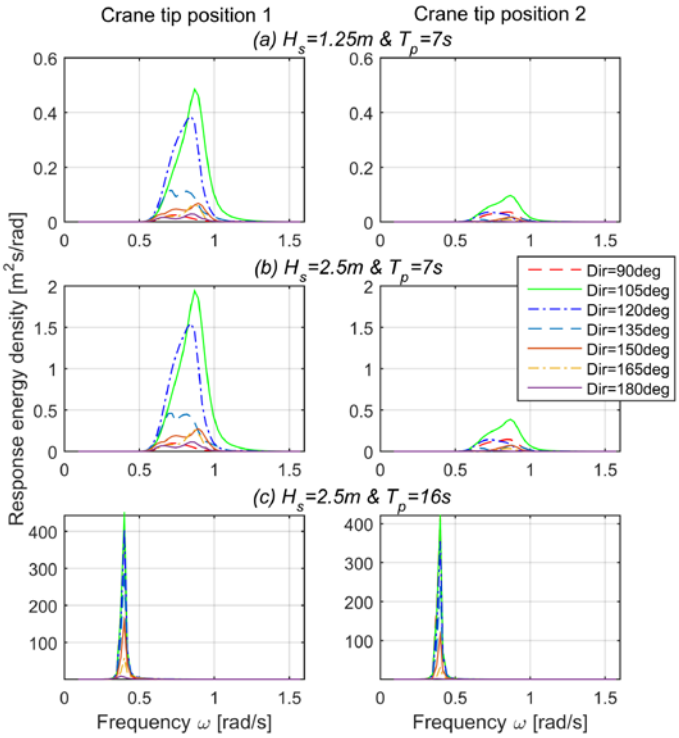

Figure 3. Response spectra of crane tip vertical motion under three wave conditions.

4.3. Limiting sea states prediction based on the limited vertical motion of crane tip

The limiting value of the crane tip vertical motion within one hour, Z_{lim} in equation (12), is assumed to be 0.5m. Besides, the acceptable probability of exceedance, q_{1h} in equation (13), is set to be 0.05 with moderate safety allowance. Moreover, it is assumed that the heavy lift operation in this study cannot be carried out under wave conditions with H_s more than 2.5m, which is believed reasonable for such operations.

Figure 4 shows the predicted limiting sea states in different wave heading directions based on the crane tip Position 1. It can be found that the acceptable H_s lowers down dramatically with increasing T_p from 6 s to 15 s. Take the wave heading Dir=165 deg for example, sea states with 2.5m H_s can be tolerated in short waves (e.g., $T_p = 6\ s$), while the acceptable Hs is smaller than 0.5m in the waves with $T_p > 10\ s$. In addition, the limiting sea states depend strongly on the wave headings. It is obvious that the limiting sea state curve becomes lower and lower from the head sea (180deg) to the more oblique sea (from 165deg to 150deg). The lower limiting sea states in the oblique sea result from the larger crane tip responses (spectrum) as shown in Figure 3 due to the influence of vessel roll motions. Specifically, the allowable H_s lowers down from around 1.8m in the wave direction 180deg to about 1.1m in the direction 150deg at $T_p = 7s$. It verifies the importance of the orientation of the vessel relative to the wave direction.

Figure 5 shows the predicted limiting sea states with varying crane tip positions in the wave heading Dir = 165 deg. It is strikingly clear that much severer sea states can be tolerated using crane tip Position 2. It echoes the previous analysis and the judgement that the motion response can be greatly mitigated by locating the crane tip toward mid-ship (closer to the CoG of the vessel).

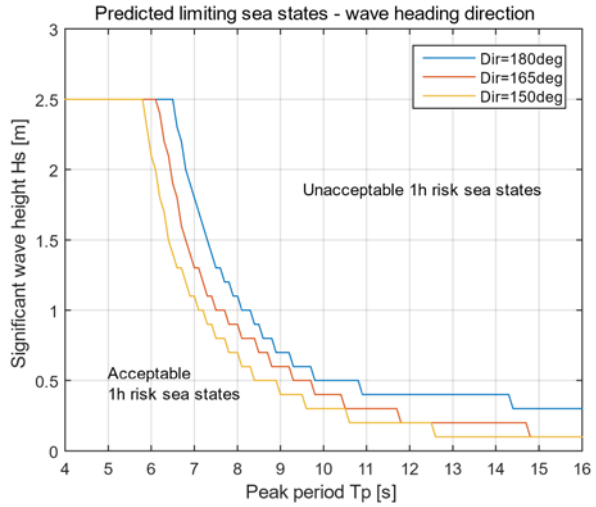

Figure 4. Predicted limiting sea states using three wave headings.

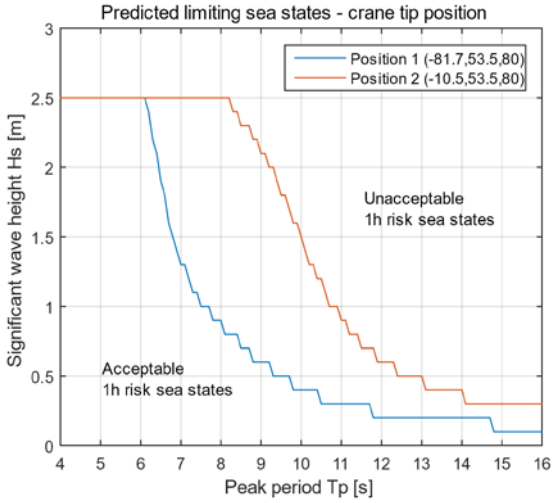

Figure 5. Predicted limiting sea states using two crane tip positions with wave heading Dir = 165°

5. Modelling of the coupled system

Numerical modelling and simulation are carried out using the software SIMA SIMO developed by SINTEF Ocean. SIMO is a non-linear time domain simulation program used for the analysis of rigid body motions and multibody systems [13] [14]. Installation of offshore support structures can be generally divided into the phases, lift-off, lowering (through wave zone) and landing on seabed. This study focuses on two phases, the lowering and the lift-off.

5.1. General setup of the lifting system

The lifting system mainly comprises of two rigid bodies, a floating vessel and a tripod foundation. Onboard the floating vessel, a rigidly connected crane has been modelled. The two rigid bodies are linked through the lift wire which extends from a winch on the crane to the top of the tripod via the crane (boom) tip. For simplicity, hook or sling wires are not modelled. Moreover, a fender coupling is modelled to hold the weight of tripod ahead of the onboard lift-off operation. Figure 6 shows the numerical model for the simulation of lowering process.

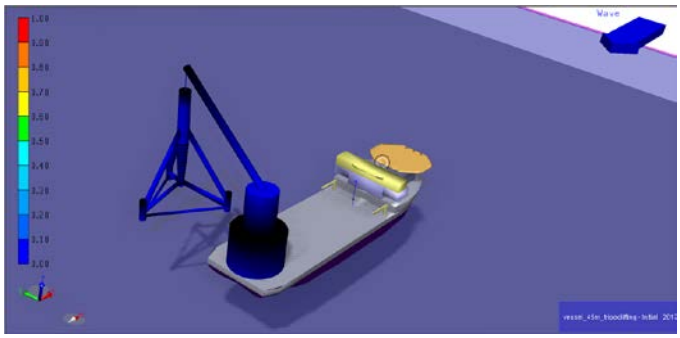

Figure 6. Numerical model for the simulation of lowering process.

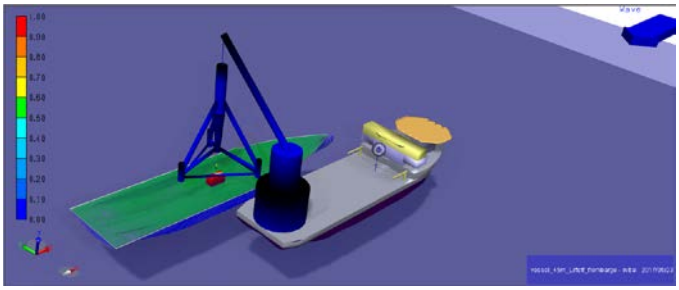

Figure 7. Numerical model for the simulation of lift-off from a barge.

For the scenario of lift-off from a transport barge, three rigid bodies are involved. In this case, wire coupling would be applied between the HLV and the tripod while fender coupling would be placed between the tripod and the barge. Figure 7 shows the numerical model for the simulation of the lift-off from a barge.

5.2. Force model on the HLV

The hydrodynamic forces on the vessel include the first order wave excitation forces, the mean wave drift forces and slowly varying forces. Waves are considered as main factor, excluding wind or current forces. The mooring system are simplified by adding linear stiffness terms in surge, sway and yaw by assuming the natural period in the three DOFs equal to 70s which is assumed reasonable for the subject HLV. Then, the stiffness, K, could be obtained following the equation [15]:

$$K_{ii} = \left(\frac{2\pi}{T_{i0}}\right)^2 \cdot (m_{ii} + A_{ii}) \, , i = 1,2,6 \tag{16}$$

where, T_{i0} is the natural period for the i^{th} DOF and $T_{i0} = 70s$, m_{ii} and A_{ii} are the mass and potential added mass, respectively.

Normally, water ballasting is performed in practice to counter the overturning moment from the lifted tripod. For simplicity, constant specified moment is introduced in the simulation of the lowering process. For the case lift-off from a barge, time dependent ballasting is applied, considering the complex relative motion between the two floating vessels.

5.3. Force model on the tripod

For slender body with the ratio between its diameter and the wave length less than 0.2, Morison's formula can be used to calculate the hydrodynamic forces. Member structures of the tripod can be modelled in slender element for the sea states concerned with T_p in the range from 5s to 12s, after checking of the corresponding wave lengths. In the slender body approximation, effects of diffraction and radiation are considered insignificant. The normal force on a moving structure in waves using Morison's formula is as follows,

$$\mathrm{f_N}(t) = -\rho C_A A\ddot{r} + \rho C_M A\dot{v} + \frac{1}{2}\rho C_D D(v - \dot{r})|v - \dot{r}| \tag{17}$$

where, v and $\dot{v}$ are fluid particle velocity and acceleration respectively; $\dot{r}$ and $\ddot{r}$ are the sectional velocity and acceleration of the moving structure; D and A are the diameter and cross-section area of structure section; C_M, C_A and C_D are the mass, added mass and drag force coefficients respectively.

C_A and C_D are dependent on many parameters such as the Reynolds number (Re), the Keulegan-Carpenter number (K_C) and the surface roughness ratio (Δ). Outer surface of the newly fabricated foundation can be assumed to be smooth. With Re in the magnitude of 10^6, combined with a small Kc number, the quadratic drag coefficient can be chosen as $C_D = 0.7$ [7].

For cylinders in unbounded fluid with a small K_c, C_A can be assumed to be independent of K_C number and equal to the theoretical value $C_A = 1.0$ for both smooth and rough cylinders [16]. However, the tripod is made of bottomless tube structures with diameters in the order of meters. Following the lowering process, the bottomless hollow structure members will be flushed with sea water following the submergence. The water inside the hollow structure affects the hydrodynamic coefficients and excitation

force on the structure members. Referring to the study on monopile lifting operation [7], $C_M = C_A = 1.8$ is applied for all the bottomless tube structures of the tripod. In addition, the slamming forces which can be calculated based on the change of the added mass with time and the relative velocity between the slender element and the wave particle motion, are omitted in the time domain simulations.

5.4. Mechanical couplings

5.4.1. Simple wire coupling. In the numerical model, the lift wire connecting the crane and the tripod is modelled as a simple wire coupling. The simple wire coupling is modelled as a linear spring according to [13]:

$$\mathrm{T} = \mathrm{k} \cdot \Delta\mathrm{l} \tag{18}$$

where T is the wire tension, K is effective axial stiffness and the Δl is the wire elongation. The effective axial stiffness, K, is given by:

$$\frac{1}{\mathrm{k}} = \frac{\mathrm{l}}{\mathrm{EA}} + \frac{1}{k_0} \tag{19}$$

where E is the modulus of elasticity, A is the cross-section area, l is the un-stretched wire length and the $1/k_0$ is crane flexibility. Material damping is set to be 2% of the EA value [13]. Table 3 lists the main parameters of the simple wire coupling.

Table 3. Main parameters of the simple wire coupling.

Lift wire properties		
Flexibility [m/N]	Damping [Ns]	EA [N]
2.00E-09	1.58E+08	7.91E+09

5.4.2. Fender coupling. A fender is defined as a contact element between the tripod and the vessel for the simulation of the lift-off operation. It can give a compressive force normal to the defined sliding plane (freeboard deck of the vessel) and a friction force along the sliding plane. In the model, the fender induced normal force acts upwards to counter the weight of the tripod. As shown in the Table 4, the friction coefficients are chosen based on empirical data between steel and steel. The normal and shear stiffness are decided based on empirical assumption.

Table 4. Main parameters of the fender coupling.

Characteristics of the fender plate				
Friction coefficient		**Shear stiffness**	**Normal stiffness**	**Internal**
Dynamic	Static	**[N/m]**	**[N/m]**	**damping [Ns/m]**
0.42	0.78	4.68E+07	6.00E+07	1.20E+06

The compressive normal force can then be found by interpolation, from a specified relation between distance and force and from the specified internal damping [13]. Linear interpolation is applied for the relationship between the distance and the normal force and it is assumed reasonable to set the internal damping as 2% of the equivalent stiffness in the normal direction.

6. Time domain simulations

6.1. Simulation of stationary process

The calculated limiting sea states in the frequency domain can only be treated as preliminary assessments since it is carried out based on the vertical crane tip motion from the decoupled HLV. Thus, the calculated limiting sea states in the frequency domain should better be verified by time-domain analysis. Table 5 shows the predicted limiting sea states from the frequency domain analysis, in the wave heading Dir=165deg, which are extracted from the results in Figure 4.

Table 5. Predicted limiting sea states in the wave heading Dir=165deg.

	Predicted limiting sea states with serial number					
	1	2	3	4	5	6
Tp [s]	5	6	7	8	9	10
Hs [m]	2.5	2.5	1.3	0.9	0.6	0.4

Stationary time-domain simulations for the predicted limiting sea states are conducted with the tripod located at two positions, one hanging in air with 13m clearance from the sea level and the other located at 5m above the sea bed (40m in draft). To account for the variability of the stochastic irregular wave conditions, 20 realizations (seeds) of 1-hour simulations for each sea state have been performed. Then, the 1-hour extreme crane tip vertical motions from different seeds are fitted into Gumbel distributions for further assessment.

Figure 8 shows the 95% quantile of the crane tip extreme vertical motion from the fitted Gumbel distribution under the predicted limiting sea states (see Table 5). This quantile corresponds to the acceptable probability of exceedance, $q_{1h} = 0.05$ used in the frequency domain analysis. It can be observed that the simulation results are generally not in line with the predictions by the frequency domain analysis, especially in the case with tripod submerged. For the seas states 1 to 3 with low peak period (from 5s to 7s), the simulated crane tip extreme vertical motions are more violent than the prediction in frequency domain for both the tripod positions, because of the resonance of the coupled system around the T_p range. The resonance mode is dominant by the tripod rotational motions, which cannot be considered from the frequency-domain analysis with HLV alone. It suggests that the predicted limiting sea states in frequency domain have been overestimated. For the sea states 4, 5 and 6 (with T_p equal to 8s, 9s and 10s, respectively), the simulation results quite agree with the frequency domain prediction in the case tripod hanging in air. However, the results are much lower when the tripod is 40m submerged due to the extra damping from the submergence. Moreover, in the submerged case, the simulated most extreme vertical motions are still lower than the pre-set limiting value 0.5m in the sea states 5 and 6, which signifies the underestimate of the limiting sea states in the frequency domain analysis. Hence, the decoupled frequency domain analysis may be used for preliminary assessment of limiting sea state, but it would incorporate some inaccuracy due to the neglecting of the coupling effects of the lifting system.

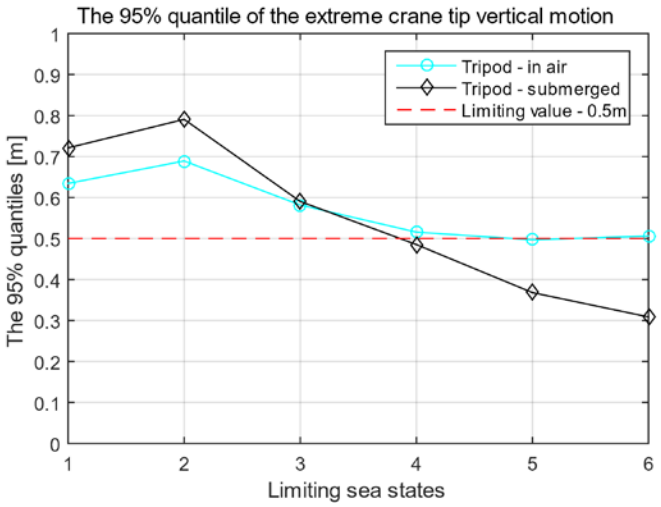

Figure 8. The 95% quantile of the crane tip extreme vertical motion under the predicted limiting sea states.

6.2. Simulation of lowering process

During the nonstationary lowering process, more critical responses (lift wire tension and tripod motions) may occur due to the nonlinear wave loads. Performance of the coupled system is investigated in the wave conditions with H_s of 2.5m, wave direction of 180°, and varying T_p. While, the focus is on the

wave condition with $T_p = 7s$, since it is of high probability of occurrence based on the wave data scatter diagram of the reference site. It should be mentioned that the wave conditions here are selected independent of the prediction in frequency domain.

Winch speed of 0.05 m/s is used. During the lowering phase, the winch runs from 300s until 1400s, equivalent to 55m wire releasing, which will lower the tripod from 13m above still water level until 3m above sea bed (42m in draft). Combined with steady state phases with 300s before and after the winch respectively, the length of each simulation is 1700s.

In time domain simulation, the time step shall be set sufficiently small to capture the highest resonant frequency of the system. To capture one cycle of phenomena in the time domain, about 15 time-steps are required [15]. With the natural period of the coupled system in the range of 0.8s to 82s (through eigenvalue analysis), the time step is supposed to be no more than $0.8/15 = 0.06$. It is set to be 0.02s for all the simulations.

6.2.1. Convergence study. Compared to the stationary simulation, the lowering process is subjected to transient effects due to nonlinear wave loads [12]. To verify the convergence of the simulations, 30 different realizations (random seed number) are performed. The extreme motions and responses from each seed are compared with the mean value of all the 30 samples. Besides, a cumulative averaged value for seed number i (the mean value from seed 1 to i), indicating the speed of convergence [15], is calculated.

Figure 9 shows an example of the convergence in the lowering phase from 30 random seeds. The main responses include the lift wire tension and the rotational motions (pitch and roll) of the tripod. It can be seen from the figure that 30 seeds are sufficient to obtain convergent results (with the cumulative average in line with the mean of the sample) for the extreme responses concerned.

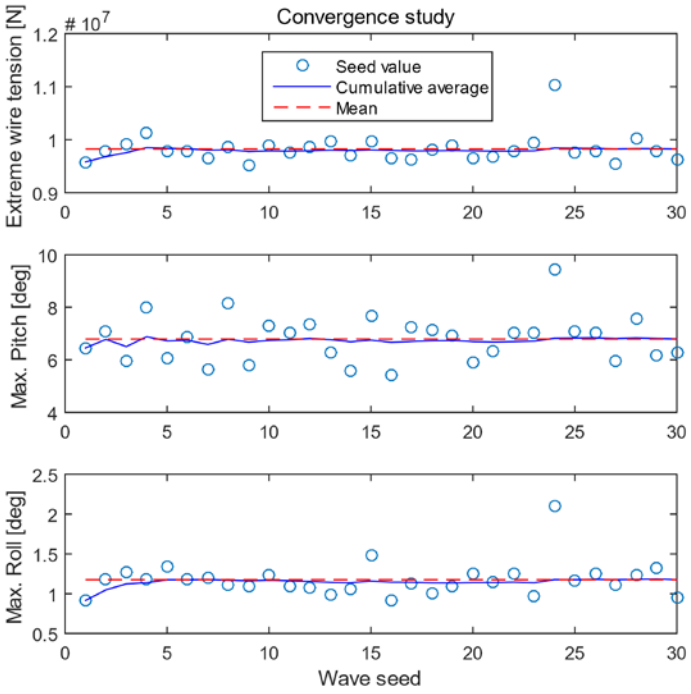

Figure 9. Convergence test results ($H_s = 2.5m, T_p = 7s$ and $Dir = 180°$).

6.2.2. Critical motions of the tripod. Besides the rotational motions, the offset of the tripod lower tips (lower end of the tripod legs) is also of concern, especially the lower tip adjacent to the hull of the vessel (see Figure 1). For the tripod, slight rotation may lead to large horizontal displacement at its lower tip due to the large size of the structure. To guarantee a safe clearance from the vessel during the lowering and ensure precise landing for smooth installation, large tip motions should be avoided.

Figure 10 shows an example (seed 2) of the critical motions of the tripod during the lowering process. Large fluctuations can be observed for the lower tip motions in X direction prior to the submergence (up to around 600s) of the tripod due to the large pendulum motions in air. However, it is damped out following the submergence into water, and the amplitude tends to stabilize until approaching the critical-draft region where the tripod motions are excited [17]. The Y-offset at the lower tip determines the safe clearance from the HLV to avoid potential collisions. Whereas, the results of the tip motion in Y direction are far away from the truth due to the application of the constant specified moment on the HLV. As clarified, specified moment has been applied on the HLV to counter the overturning moment from the hanging tripod. Although equilibrium of moment is guaranteed in air based on the dry weight of the tripod, the balance is broken once the tripod dips into the waves. Following the submergence of the tripod, the decreasing wet weight of the tripod results in the overbalance of the specified moment, which causes continuous positive rolling of the HLV and consequently leads to the abnormal motions of the tripod. In this study, the tripod is originally positioned 8m away from the portside of the vessel, far enough to avoid any collision. But rather than the specified moment, time dependent ballasting is recommended for the future study to avoid the unwanted motions.

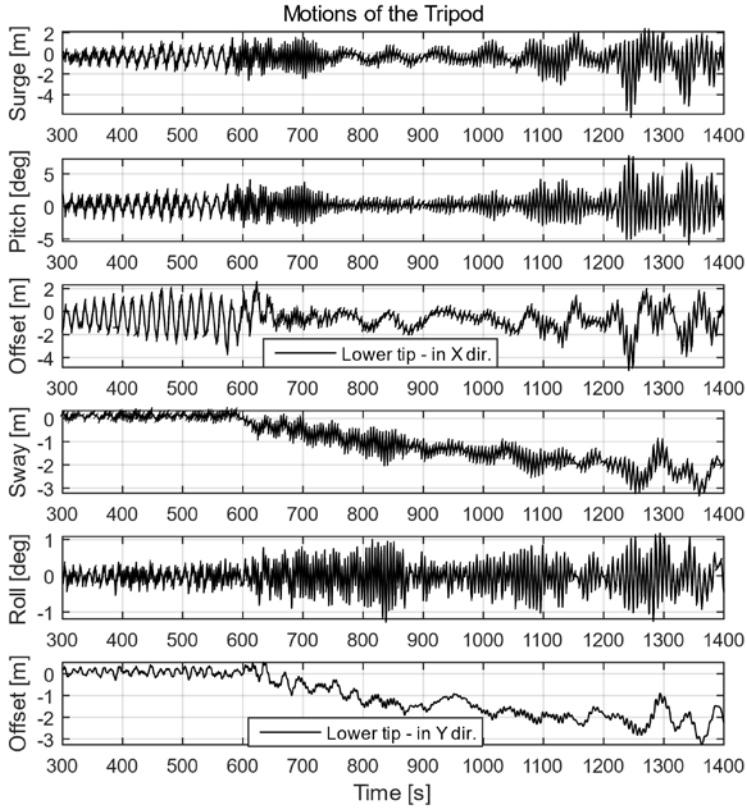

Figure 10. Critical motions of the tripod during the lowering process ($H_s = 2.5m, T_p = 7s$ and $Dir = 180°$).

6.2.3. Influence from the vessel type. Compared to the floating HLV, a jack-up vessel acts as a bottom-fixed structure and provides a stable working platform.

Figure 11 shows an example of the time series of tripod motions and the lift wire tension using the HLV and a jack-up. Compared to the large pitch and tip motion in air using the HLV, no vessel motions are transferred to the tripod from the bottom fixed jack-up vessel. After entering into water, the pitch motions are consistent for the two cases as the lowering continues which suggests that the motions of the tripod are then more affected by the wave forces than the vessel motions. Different from the case using the HLV, there are hardly any roll motion on the tripod using the jack-up, thanks to the long crested, head sea wave condition and the stillness of the jack up vessel. Consequently, the larger roll motion of tripod when using the HLV leads to larger dynamic tension force in the lift wire. Meanwhile,

the transversal offset of the tripod lower tip (using the HLV) is also more critical than the case using the jack-up.

Figure 12 shows the statistical maximum lift wire tension and maximum rotational motions of the tripod under the sea states with varying T_p by using two vessels. It can be observed that the rotational motions of the tripod and the tension in the lift wire are smaller by using the jack-up, especially in the long waves. The deviations from the vessel type are enlarged in the long waves with T_p around 11s and 12s, because of increasing motions of the HLV in long waves as the wave peak period approaches to the eigenperiod.

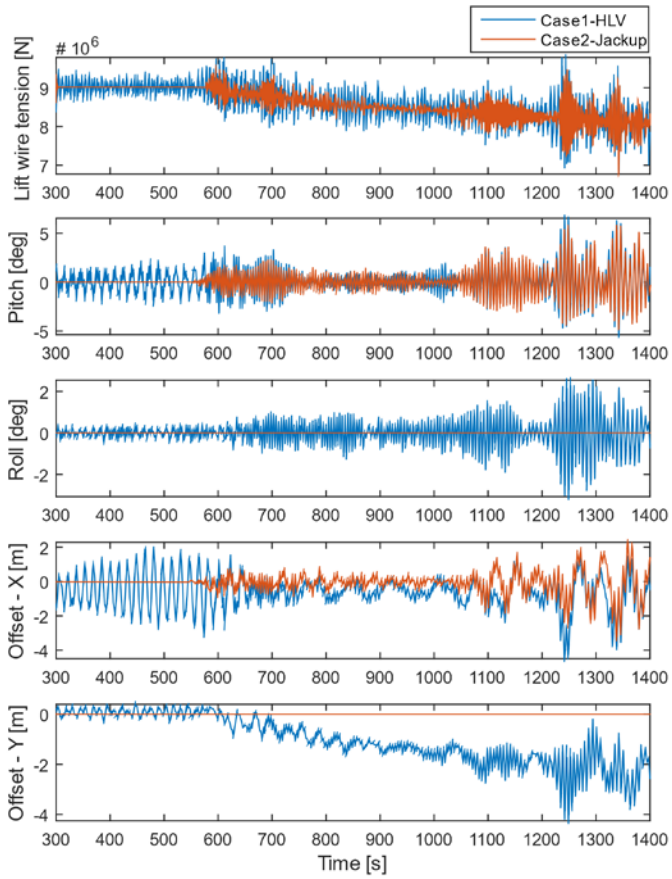

Figure 11. Time series of the lift wire tension and the tripod motions by using different vessels ($H_s = 2.5m$, $T_p = 7s$ and $Dir = 180°$).

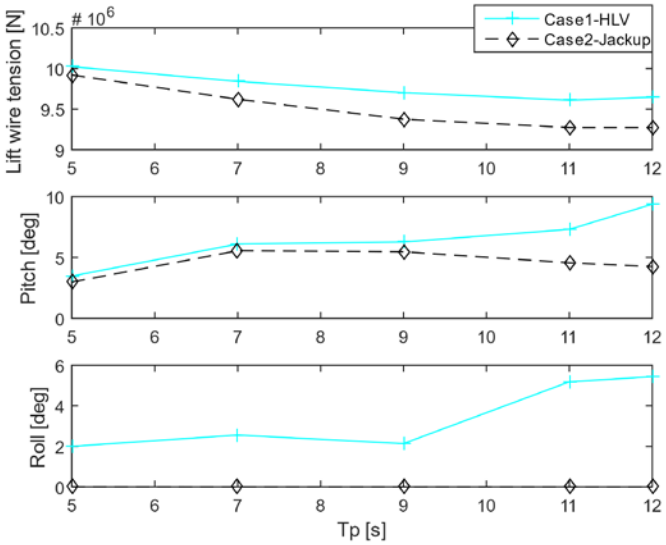

Figure 12. Statistics of extreme responses under various T_p by using different vessels ($H_s = 2.5m$ and $Dir = 180°$).

6.3. Simulation of lift-off operation

Lift-off operation is critical, and many hazards may occur, such as snap loads in lift wire, unacceptable horizontal offset of object following the lift off or even re-hit after lift-off from a barge. To study this critical lifting phase, two cases, lift-off from its own deck and lift-off from a barge, are investigated by performing time-domain simulations. In this study, the barge is modelled with the same hydrodynamic characteristics as the crane vessel (HLV). They are positioned side by side, both heading against the wave. Varying hoisting speeds from 0.1m/s [10] are investigated for the case onboard lift-off.

The winch starts from 200s. It firstly pays in the pre-set loose wire (1.5m) which is long enough to accommodate the relative motion between the crane tip and the seated tripod. The winch is kept engaged until the tripod is lifted 5m upward from its original sitting position. The total length of the dynamic simulation is set to be 450s, so that the system would stay in steady state for certain period after the winch stops.

6.3.1. Lift-off from the deck of the HLV. The simulation of the onboard lift-off is firstly carried out with the winch speed of 0.1m/s, under the sea state $H_s = 2.5m, T_p = 7s$ and $Dir = 180°$. No severe surge or pitch motion are observed, not to mention the negligible sway and roll in the head sea. Thus, attention is brought to the extreme tension force in the lift wire during the operation.

Figure 13 shows the time history and the statistical maximum tension forces in the lift wire during the onboard lift-off with various hoisting speeds. It should be noted that the fluctuation of the wire tension force due to the stop of the winch which is not of concern in this study, has been filtered out. It turns out that the lift-off of the tripod from the deck of the HLV can be smoothly carried out without any slack wire for all the hoisting speeds concerned. Higher peak can be observed with larger hoisting speed, especially when the speed is increased from 0.4m/s to 0.5m/s. Hence, it is critical to control the hoisting speed during the lift-off.

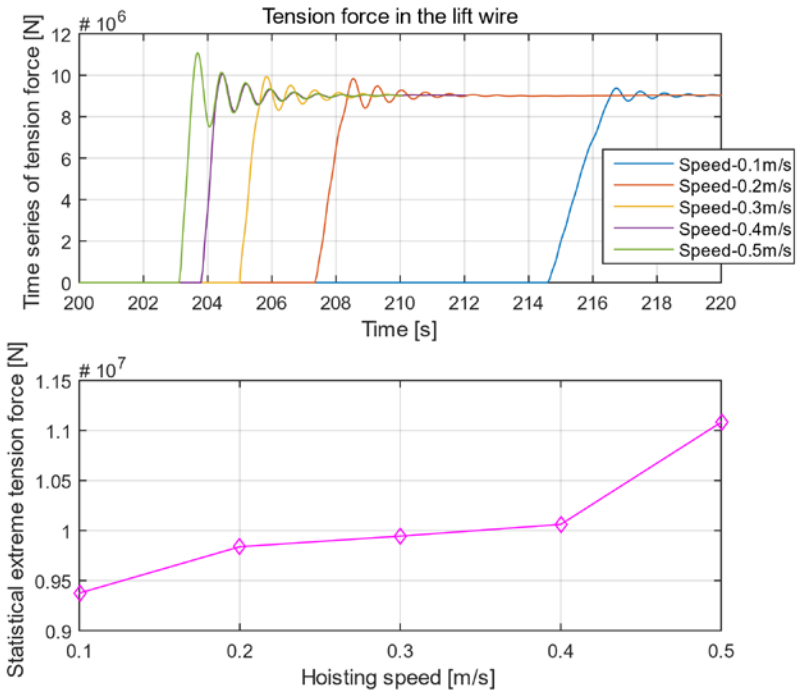

Figure 13. Time series and statistical maximum tension force in the lift wire w.r.t. hoisting speeds ($H_s = 2.5m, T_p = 7s$ and $Dir = 180°$).

6.3.2. Lift-off from a transport barge. Due to the increase of complexity of the coupled system by adding the barge, more wave seeds may be needed for the time-domain simulations to reach a reasonable convergence [18]. After convergence test, it turns out that 45 seeds of time-domain simulations for each sea state are sufficient to achieve convergent results for the extreme lift wire tension.

The process in this case is much more violent compared to lift-off from the own deck of HLV, and high peaks of the coupling forces can be observed as shown in Figure 14. The results are selected from two seeds, seeds 22 and 39 corresponding to the extreme and the moderate situations from the convergence test. The peaks of the lift wire tension are snap loads following the slack in the lift wire. The snap load in the extreme wave seed (seed 22) is almost twice as large as the normal wire tension during hanging in the steady state after successful lift-off. It is the reason that slack slings or wires are recommended to be avoided [10] [19]. Although same settings as the onboard lift-off are applied in this simulation, such as the loose wire length (1.5m) and winch speed (0.1m/s), the lift wire gets stretched as early as 210s with few seconds earlier than the onboard lift-off. It is the result of the relative motions between the HLV and the barge. During the first load transfer, amplitude of the snap force can reach almost the level of the normal wire tension during hanging in steady state. Following the consequent slack-wire cases, the snap load further increases until the tripod is successfully lifted off. The peaks of the fender force also increase following each slack-wire until the lift-off is completed.

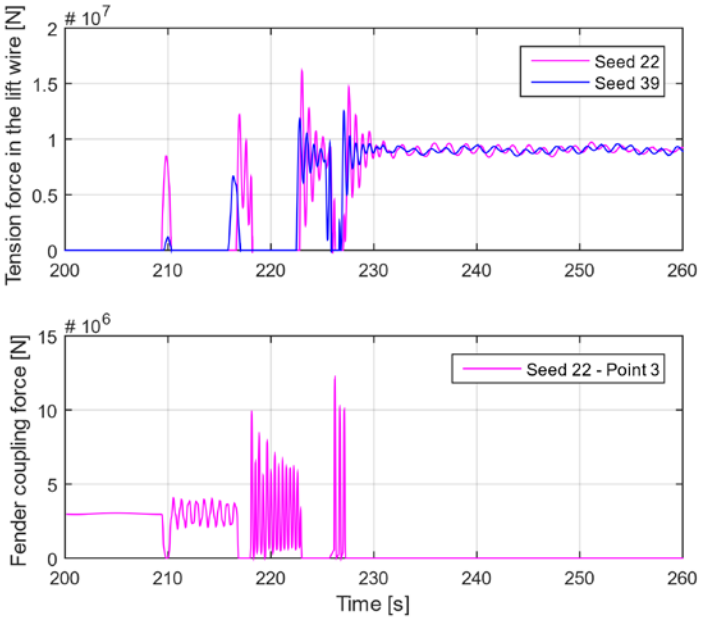

Figure 14. Time series of the coupling forces ($H_s = 2.5m, T_p = 7s$ and $Dir = 180°$).

Regarding the motions of the system during lift-off, the whole process can be divided into three phases. Phase one lasts until the lift wire gets taut (around 209s). The dynamic system can be treated as two separate systems, the barge with tripod seated on and the floating HLV. Phase two is the continuous lifting until the successful lift-off (until around 227s). The last phase refers to the consequent steady state hanging in air which also comprises of two separate systems, the free barge and the HLV with the lifted tripod. Slack and re-hit occurs during phase two.

Figure 15 shows the critical motions of the tripod during the lift-off from a barge. In the first phase, the motions of the tripod are similar as those of onboard lift-off. In this phase, little roll or sway can be observed due to the head sea condition, which contributes to the near-zero tip motion in Y direction. On the other hand, small pitch and surge motions occur which leads to few tip motions in X direction. During phase two, tripod motions become bigger but still moderate. Attention is brought to the motions immediately after the successful lift-off. Large tripod motions can be observed, followed by noticeable tip motions in both X and Y direction. Even with time dependent ballasting system, significant motions would be involved on the HLV due to the transfer of the heavy load (the tripod). In this case, more attention shall be paid to verify the safety clearance to avoid the collision.

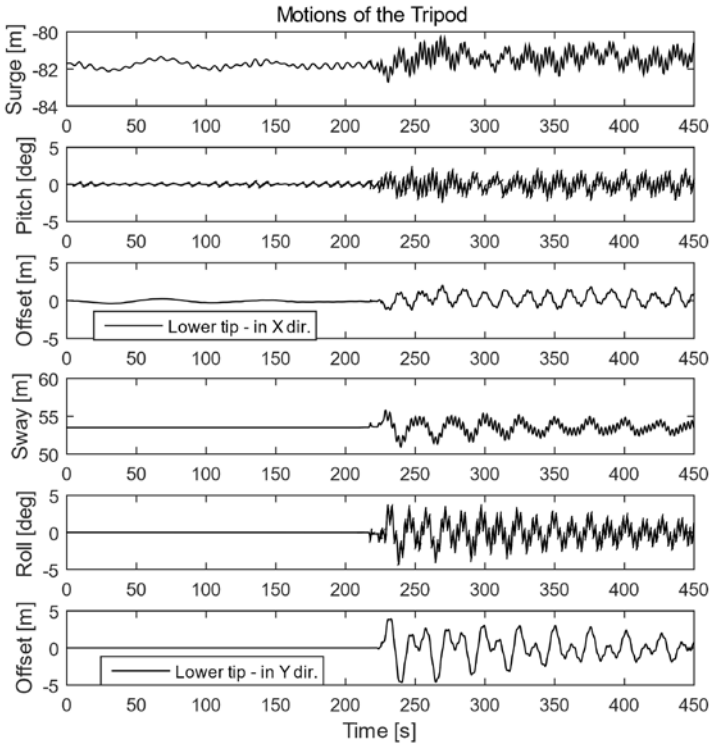

Figure 15. Critical motions of the tripod ($H_s = 2.5m, T_p = 7s$ and Dir=180°).

Compared to the onboard lift-off with minor motion responses, lift-off from a barge is much more demanding, accompanied by critical snap load and significant motion responses.

7. Conclusions

The installation of a tripod foundation using a heavy lift vessel (HLV) was investigated in this study. The limiting sea states were firstly calculated in the frequency domain and later verified in the time domain. In frequency domain analysis, case studies were included using different wave directions and crane tip positions. Then, numerical modelling and time-domain simulations of the coupled dynamic system during the lowering phase and the lift-off phase were performed. For the lowering phase, comparative studies using two types of installation vessel, the HLV and the Jack-up, were investigated. For the lift-off phase, two scenarios, lift-off from the own deck of the HLV and lift-off from a transport barge were studied. Besides, case study on various hoisting speeds during the onboard lift-off was also presented.

Based on the investigations, some essential findings can be summarized in the following:

1) The crane tip vertical motion can be greatly mitigated by locating the crane tip toward the mid-ship and consequently severer sea states can be tolerated. Rougher sea states can also be tolerated by aligning the lifting vessel in the head sea rather than in oblique waves.
2) The predicted limiting sea states using frequency domain method is found inappropriate due to the neglecting of the coupling effects of the lifting system. The calculated limiting H_s were overestimated in short waves but underestimated in long waves compared to the time-domain results with tripod submerged in 40m draft.
3) The vessel type has significant impact on the system responses. Both the wire tension and the tripod motions are smaller by using the jack-up. Especially during the lowering in air, barely any tripod motions occur when using the jack-up.

4) Compared with the onboard lift-off, there are much more challenges for the lift-off from a barge. Under the considered wave condition, the onboard lift-off operation can be smoothly performed while the lift-off from the barge experiences critical snap load and violent tripod motions.

Taking into consideration the simplifications in the present numerical models, recommendations for future work are discussed as follows:

1) Shielding effects from the HLV on the responses of the tripod should be taken into consideration. The simulations in this study were carried out in the undisturbed waves. Referring to the investigation [7], shielding effects may be significant especially in short waves.
2) The effects from wave spreading (short crested wave) should be considered. This study was conducted in long crested, head sea wave condition for the nonstationary time domain simulations. It may result in non-conservative results, especially the roll related motions.

References

[1] WindEurope 2017 *The European offshore wind industry – key trends and statistics 2016* (windeurope.org)

[2] IEA 2013 *Technology roadmap: Wind energy*. URL: http://www.iea.org/publications/freepublications/publication/Wind_2013_Roadmap.pdf. [Accessed 02 02 2017]

[3] Gao Z, Acero W G, Li L, Zhao Y, Li C and Moan T 2016 Numerical simulation of marine operations and prediction of operability using response-based criteria with an application to installation of offshore wind turbine support structures *Proc. Marine Operations Specialty Symp. (MOSS2016)* singapore

[4] Haver S 2007 *Prediction of characteristic response for design purposes report (Draft version)*

[5] Li L, Acero W G, Gao Z and Moan T 2016 Assessment of allowable sea states during installation of offshore wind turbine monopiles with shallow penetration in the seabed *Journal of Offshore Mechanics and Arctic Engineering* vol 138(4) 041902

[6] Xu D 2016 *Numerical modelling and simulations for lowering of an offshore wind turbine tripod (Master thesis)* (Trondheim: Norwegian University of Science and Technology)

[7] Li L, Gao Z, Moan T and Ormbrg H 2014 Analysis of lifting operation of a monopile considering vessel shielding effect *Marine Structures* vol 39 pp 287-314

[8] Li L, Gao Z and Moan T 2015 Joint distribution of environmental condition at five European offshore sites for design of combined wind and wave energy devices *Journal of Offshore Mechanics and Arctic Engineering* vol 137 no 3

[9] Faltinsen O M 1990 *Sea loads on ships and offshore structures* (Cambridge: Cambridge University Press)

[10] DNV 2011 *Recommended Practice DNV-RP-H103, Modelling and analysis of marine operations* (Det Norske Veritas)

[11] Haver S 2016 *Marine Operations (lecture notes)* (Stavanger: University of Stavanger)

[12] Li L, Gao Z and Moan T 2016 Operability analysis of monopole lowering operation using different numerical approaches *Int. Journal of Offshore and Polar Engineering (ISSN 1053-5381)* vol 26 no 2 pp 88-89

[13] MARINTEK 2016 *SIMO Theory Manual (Version 4.8.2)* (MARINTEK)

[14] MARINTEK 2016 *SIMO User Guide (Version 4.8.2) (*MARINTEK)

[15] Li L, Gao Z and Moan T 2013 Numerical simulations for installation of offshore wind turbine monopiles using floating vessels *ASME 2013 32nd Int. Conf. on Ocean, Offshore and Arctic Engineering* Nantes

[16] DNV 2011 *Recommended Practice DNV-RP-C205, Environmental conditions and environmental loads* (Det Norske Veritas)

[17] Birkeland F M 2016 *Numerical Simulation for Installation of XL Monopile for Offshore Wind Turbine (master thesis)* (Trondheim: Norwegian University of Science and Technology)

[18] Acero W G, Gao Z and Moan T 2015 Assessment of the dynamic responses and allowable sea states for a novel offshore wind turbine installation concept based on the inverted pendulum principle *Energy Procedia* vol 94 pp 61-71

[19] Sarkar A and Gudmestad O T 2010 Splash zone lifting analysis of subsea structures *ASME 2010 29th Int. Conf. on Ocean, Offshore and Arctic Engineering* pp 303-312

[20] Mavrakos S 1988 Hydrodynamic coefficients for a thick-walled bottomless cylindrical body floating in water of finite depth *Ocean Engineering* vol 15 no 3 pp 213-229

[21] Baar J J M, Pijfers J G L and Santen J A 1992 Hydromechanically coupled motions of a crane vessel and a transport barge *Proc.Offshore Technology Conf.* (Houston:Offshore Technology Conferene)

[22] Li L, Gao Z and Moan T 2015 Response analysis of a nonstationary lowering operation for an offshore wind turbine monopile substructure *Journal of Offshore Mechanics and Arctic Engineering* vol 137 no 051902